Optimal Contact Decisions for Ergodic Exploration

Lauren M. Miller, *Student Member, IEEE,* and Todd D. Murphey, *Member, IEEE,*

***Abstract*— This paper presents a method of determining optimal contact transition times for a surface exploration task. A transition time optimization algorithm is developed which uses a measure of ergodicity as the objective function, requiring the time-averaged dynamics of the system to optimally approximate the spatial average of a distribution on a finite time interval. This approach is demonstrated to be effective for determining a finite number of contact transition times in a computationally efficient way. The approach is generalized to include a measure of energy loss during sampling modes. The algorithm is shown to result in solutions that are qualitatively similar to the observed behavior of human subjects performing feature localization tasks.**

I. Introduction

Humans are particularly adept at identifying objects using tactile information [1]. Several studies in psychology have attempted to characterize human tactile exploratory behavior in order to motivate control techniques that operate using similar principles [1]–[3]. Notably, Lederman and Klatzky experimentally demonstrated that human tactile exploration can be described by a sequence of distinct exploratory procedures (EPs), dependent on the sensing task. For example, object enclosure is typically used for extracting gross-level shape, and surface scanning is used for feature localization and identification [3].

In addition to being naturally described by switching between a discrete set of high-level modes, tactile exploration is also characterized by making and breaking contact with an object or surface. Huynh, Stepp et. al demonstrate that during feature localization, the exploration strategy used by human subjects switches from continuous scanning to ballistic motion followed by local exploration if the subject has previous experience with the task [2]. This suggests that the sensing strategy chosen reflects whether or not a subject has an internal expectation of the location of a feature.

The aim of this paper is to derive a mathematical algorithm for determining when mode transitions (e.g. when to make and break contact) should occur for the example of a surface feature localization task. Motivated by observations of human exploratory behavior, this algorithm explicitly takes into account a probabilistic representation of the location of the desired feature. For a localization task, this is equivalent determining which regions of the domain to sample and which to ignore.

The contact decision problem is formulated as a transition time optimization problem. The objective function for the optimization uses the principle of ergodicity to quantitatively assess how well a spatial distribution is being sampled, averaging the trajectory of a sensor over time. A generalized method for including a measure of energy loss during sampling modes was examined as well. Several simulations are performed using this method. These results are shown to be qualitatively similar to behavior observed in human subject experiments.

The authors are with the Department of Mechanical Engineering, Northwestern University, Evanston, IL, 60208 USA (e-mail: LaurenMiller@U.Northwestern.edu, T-Murphey@Northwestern.Edu

A. Related Work

Numerous studies have been devoted to reconstructing surfaces or objects in three dimensions [4]–[8], and identifying surface features [9] from tactile information. Most of these strategies assume some variation of regular or uniform sampling; there has been a relatively little work done on designing efficient control strategies to drive tactile data collection. In [6] an algorithm is developed to match 3D objects to a known database that uses an interpretation tree method to select the optimal next sensing move from a set of primitives, but does not allow ballistic motion. A method is proposed in [10] which uses a residual hull method for 3D object recognition, choosing a movement that reduces the difference between an initial enveloping polyhedral model and the hull defined by a discrete set of contact points at each point in space. Mathew and Mezic derive a receding horizon control strategy based on the principle of ergodicity for continuous systems [11].

While there is a great deal of work in reconstructing features or identifying objects from tactile information, there remains a lack of a method that uses a precise measure of spatial expectation to plan exploratory motion that is amenable to hybrid systems, and efficient both computationally and energetically.

II. Transition Time Optimization

Hybrid systems are those that experience discrete changes between continuous dynamic modes. A general hybrid system with N transitions can be described by a sequence of dynamic equations of the form:

$$x(t_0) = x_0, \qquad \dot{x}(t) = g_i(x(t)) \;\; \tau_i < t < \tau_{i+1} \qquad (1)$$

for $i = 1, \ldots, N$, where each $g_i(t, x)$ is a distinct dynamic mode. Transition time optimization involves determining the optimal times for transitions between these modes by minimizing an objective function. Derivations of optimization algorithms for determining switching times can be found in [12]–[14]. Hybrid optimization is a particularly compelling framework for studying exploratory behavior for several reasons. At a high level, tactile exploration can be naturally presented as a hybrid system, as it can be categorized into

distinct exploratory procedures [15]. Additionally, tactile sensing involves making and breaking contact; contact transitions are naturally hybrid.

Hybrid system optimization is also appealing from an implementation perspective. Solving for transition times between known dynamic modes is often a better-posed, better-conditioned problem than the continuous problem, in that it is only necessary to solve for a finite number of transition times. Additionally, previous work in hybrid system optimization using second-order information has shown significant decrease in computation time compared to first-order methods, which is critical for real-time calculations necessary for active sensing [12], [13], [16].

In this paper, it is assumed that the number of switches as well as the mode order is known. A method for determining the order in which mode changes occur is provided in [12]. The problem therefore reduces to solving for a set of transition times that minimize a cost function J, for a given set of modes and distribution, i.e.

$$\arg\min_{\tau} \quad J(\tau),$$

where τ is the set of transition times.

A. Optimization Methods

This paper presents derivations of the first and second derivatives of the objective function $J(\tau)$ with respect to a set of transition times, which are then used in standard first and second order iterative optimization algorithms. Gradient descent, which relies on the first derivative of the cost function with respect to the transition times, chooses a descent direction $d = -D_\tau J$, iterating until some convergence criteria has been met. Newton's method, which can improve convergence time of the algorithm in convex regions by orders of magnitude, relies on both the gradient and the Hessian to calculate a descent direction according to $d = -D_\tau^2 J^{-1} \cdot D_\tau J^T$.

In the simulations provided in section VI, a combination of gradient descent and Newton's method was used: given a set of initial transition times, the algorithm initially iterates using gradient descent, and switches to Newton's method when the Hessian is determined to be positive definite. A backtracking line search was utilized in the optimization methods shown above in order to ensure sufficient decrease. Details on the optimization algorithms can be found in [17].

B. Notation

The notation used in this paper follow [13]. Slot derivative notation is used throughout; i.e. $D_n f(arg_1, arg_2, ...)$ represents the derivative of the function $f(\cdot)$ with respect to the argument at position n. $D_{arg}(...)$ is the derivative with respect to arg. The $\circ$ operator is used to represent linear mappings, e.g. $M \circ v = M \cdot v$, and $M \circ (v, u) = v^T[M]u$.

III. Ergodicity

In order for a system to be ergodic, the fraction of time spent sampling an area should be equal to some metric quantifying the density of information in that area. This idea is expressed graphically in Fig. 1, where the distribution $\phi(x)$, depicted as level sets over the domain X, is sampled by a sensor following the trajectory $x(t)$ from $t = 0$ to $t = T$. The trajectory $x(t)$ is *ergodic* with respect to the PDF $\phi(x)$ if the percentage of time spent in any subset N of X from $t = 0$ to $t = T$ is equal to the measure of N. The equations in Fig. 1 represent the condition for ergodicity for the two subsets shown; this condition must hold for all possible subsets.

The objective for a sensing task should capture the same information; the aggregate motion of a sensor should result in more samples from the most information-dense areas of a distribution. The spatial distribution used for calculating ergodicity will vary based on the sensing task. For example, if the goal is to reconstruct a surface, a desirable distribution would be the variance of the estimated surface over the surface manifold. If the goal is to localize a feature, the distribution would be the probability that the feature is located at any point in the domain. Mathew and Mezic [11] derive a continuous time feedback controller for a sensing task that uses a metric that quantifies both the ergodicity of a system and energy expended. In this paper an algorithm is developed using the same measure of ergodicity as in [11], adapted to hybrid systems, and is shown to be computationally efficient and effective for nonlinear systems.

A. Metric for Quantifying Ergodicity

There are different ways of expressing ergodicity. In this paper, the metric presented by Mathew and Mezic will be used to calculate how far a trajectory is from being ergodic with respect to a distribution. This approach uses the distance between the Fourier basis functions of the spatial distribution and the time-averaged distribution, quantified by the weighted norm of the Fourier coefficients, as a measure of

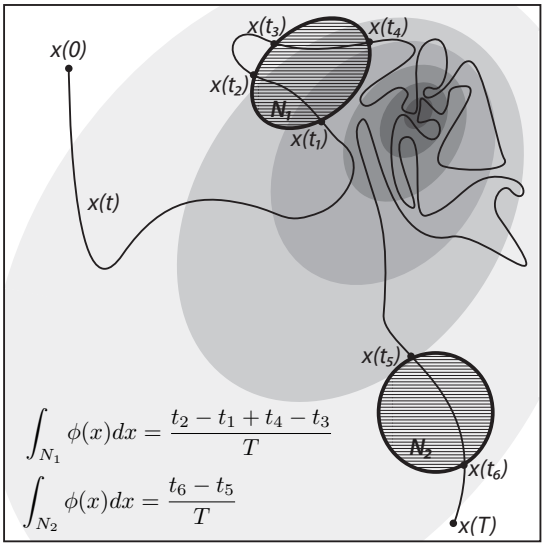

Fig. 1: Conceptual illustration of what it means for the trajectory $x(t)$ to be ergodic with respect to the distribution $\phi(x)$, represented by the level sets shown. Equations representing the condition for ergodicity for the two subsets, N_1 and N_2 are shown.

the ergodicity. A clear and thorough derivation of the metric can be found in [11]. A brief summary follows.

It is assumed there is a probability distribution function $\phi(x)$ over a rectangular region of interest $X \subset \mathbb{R}^n$ defined as $[0, L_1] \times [0, L_2] ... \times [0, L_n]$. As in [11], the Fourier basis functions that will be used, on the domain X are

$$f_k(x) = \frac{1}{h_k} \prod_{i=1}^{n} \cos\left(\frac{k\pi}{L_i} x_i\right), \text{for } k = 0, 1, 2...K$$

$$\text{where } h_k = \left(\int_X \prod_{i=1}^{n} \cos^2\left(\frac{k\pi}{L_i} x_i\right)\right)^{1/2},$$

where K is the number of basis functions used. The time-averaged trajectory can be represented as a point wise function of point $\bar{x}$ and trajectory $x(t)$ as follows:

$$C(\bar{x}, x(t)) = \frac{1}{T_f} \int_0^{T_f} \delta(\bar{x} - x(t)) dt$$

The Fourier coefficients of the basis functions along the trajectory, averaged over time, can be computed using the inner product of $C(\bar{x}, x(t))$ and $f_k(\bar{x})$, as follows:

$$c_k(x(t)) = \frac{1}{T_f} \int_0^{T_f} f_k(x(t)) dt. \tag{2}$$

The Fourier coefficients of the spatial distribution $\phi(x)$ are computed in a similar way:

$$\phi_k = \int_X \phi(x) f_k(x) dx.$$

The a measure of the distance between $C(\bar{x}, x(t))$ and $\phi(\bar{x})$, can therefore be expressed as

$$\sum_{k=0}^{K} \Lambda_k |c_k(T_f) - \phi_k|^2, \tag{3}$$

where Λ_k is a scaling factor which weights lower frequency basis functions more than higher frequency, defined according to [11], as

$$\Lambda_k = \frac{1}{(1 + ||k||^2)^s} \quad \text{and} \quad s = \frac{n+1}{2}. \tag{4}$$

While equations presented up until this point are essentially identical to [11], the following sections present a novel use of Eq. (3) in a transition time optimization framework, used to solve a different class of problem.

IV. Ergodic Objective Function

The derivation and simulations presented in this paper assume a single agent sampling along a one dimensional space, although extension to multiple dimensions and agents is straightforward. The time horizon, number of transition times, and mode order is assumed to be known in advance, as well as the PDF ϕ that represents the areas in a finite region that are of particular interest to explore, as defined in Section III-A. The system dynamics are defined as in Eq. (1).

In order to mathematically differentiate between modes during which sampling does or does not occur, it is convenient to rewrite Eq. (2) as

$$c_k(x(t), \tau) = \frac{1}{T_E(\tau)} \int_{T_0}^{T_f} \ell_k(x(t, \tau)) dt, \tag{5}$$

where

$$\ell_k = \begin{cases} f_k(x(s, \tau)) & \text{sampling modes} \\ 0 & \text{non-sampling modes} \end{cases} \tag{6}$$

Thus, although the trajectory $x(t)$ is continuous, the segments of the trajectory during non-sampling modes are not included in the calculation of the Fourier coefficients of the time-averaged trajectory. The total sampling time must also be adjusted to represent the total duration of time spent in sampling modes, defined as T_E below:

$$T_E(\tau) = T_f - \sum_{i \in N_e} (\tau_{i+1} - \tau_i). \tag{7}$$

where N_e is the set of modes during which sampling occurs. The objective function will now be defined as

$$J(\tau) = \sum_{k=0}^{K} \Lambda_k \left| \tfrac{1}{T_E(\tau)} G_k(x(t, \tau)) - \phi_k \right|^2, \tag{8}$$

where

$$\begin{aligned} G_k(\cdot) &= \int_{T_0}^{T_f} \ell_k(x(s, \tau)) ds \\ &= \int_{T_0}^{\tau_1} \ell_{k,1}(x(s, \tau)) ds + \int_{\tau_1}^{\tau_2} \ell_{k,2}(x(s, \tau)) ds \\ &\quad + \ldots + \int_{\tau_N}^{Tf} \ell_{k,N}(x(s, \tau)) ds. \end{aligned} \tag{9}$$

As will be demonstrated in the next section, the discontinuity in $\ell_k(x, \tau)$ with respect to $x(\tau, t)$ results in the transition time derivatives looking almost identical to impulse optimization [16].

V. Optimality Conditions for Ergodic Transition Time Optimization

A. First Derivative of $J(\cdot)$

Lemma 1: The first partial derivative of the cost function in Eq. (8) with respect to a single transition time τ_i can be calculated as follows:

$$\begin{aligned} D_{\tau_i} J(\cdot) &= \sum_{k=0}^{K} \Lambda_k \Big[2 \left(\tfrac{1}{T_E(\tau)} G_k(x(t, \tau)) - \phi_k \right) \circ \\ &\quad \left(D_{\tau_i} \tfrac{1}{T_E(\tau)} \circ G_k(x(t, \tau)) + \right. \\ &\quad \left. \tfrac{1}{T_E(\tau)} D_{\tau_i} G_k(x(t, \tau)) \right) \Big], \end{aligned} \tag{10}$$

where

$$\begin{aligned} D_{\tau_i} G_k(x(\tau)) &= \psi_k(\tau_i) \circ X^i + \\ &\quad \ell_{k,i-1}(x(\tau_i), \tau_i) - \ell_{k,i}(x(\tau_i), \tau_i) \end{aligned} \tag{11}$$

and $\psi_k(t)$ is the first-order adjoint found by solving the following backwards differential equation:

$$\dot{\psi_k}(t) = -D_x g(x(t))^T \circ \psi_k(t) - D_1 \ell_k(x(t),t)^T \qquad (12)$$
$$\psi(T_f) = 0.$$

X^i is defined as shown below for compactness, following [13].

$$X^i = g_{i-1}(x(\tau_i),\tau_i) - g_i(x(\tau_i),\tau_i) \qquad (13)$$

Proof: Equation (10) results from the application of the chain rule to Eq. (8). The expression for $D_{\tau_i}G_k(\cdot)$ is obtained by differentiating $G_k(\cdot)$ with respect to a transition time τ_i, applying the chain rule and the Leibniz rule to obtain

$$\begin{aligned} D_{\tau_i}G_k(\cdot) &= \int_{T_0}^{T_f} D\ell_k(x(s,\tau)) \circ D_{\tau_i}x(s,\tau)ds + \\ &\quad \ell_{k,i-1}(x(\tau_i),\tau_i) - \ell_{k,i}(x(\tau_i),\tau_i). \end{aligned} \qquad (14)$$

The partial derivative of $x(t)$ with respect to a transition time τ_i can be calculated using a state transition matrix operating on an initial condition:

$$D_{\tau_i}x(t) = \Phi(t,\tau_i) \circ X^i, \qquad (15)$$

where $\Phi(t,\tau)$ is the solution to $\dot{z}(t) = [D_1 g(x(t),t)]\, z(t)$. By Substituting Eq. (15) for $D_{\tau_i}x(t)$ into the expression for $D_{\tau_i}J(\cdot)$ above and pulling X^i out of the integral, $\psi_k(t)$ can be defined as

$$\psi_k(t) = \int_{\tau_i}^{T_f} D_1\ell_k(x(s,\tau)) \circ \Phi(s,\tau)ds,$$

which is then differentiated to obtain the expression for $\dot{\psi_k}(t)$ shown above.

The derivation of $D_{\tau_i}G_k(\cdot)$ is essentially the same as switching time optimization if $\ell_{i-1}(x(\tau_i) = \ell_i(x(\tau_i)$, or impulse optimization if $\ell_{i-1}(x(\tau_i) \neq \ell_i(x(\tau_i)$. More formal derivations of $D_{\tau_i}x(t)$ and $\psi_k(t,\tau)$ for both cases can be found in [13] and [16]. ■

The benefit of solving this problem using the backwards integration of the adjoint equation is that the cost of evaluating the gradient at each iteration of the optimization routine does not scale with the number of switching times; K adjoint equations are solved once per iteration, and evaluated at each transition time.

B. Second Derivative of $J(\cdot)$

Lemma 2: The derivative of (10) with respect to a second transition time τ_j can be calculated as follows:

$$\begin{aligned} &D_{\tau_j}D_{\tau_i}J(\cdot) = \sum_{k=0}^{K} 2\Lambda_k \\ &\Big[\Big(D_{\tau_j}\tfrac{1}{T_E(\tau)} \circ G_k(x(t,\tau)) + \tfrac{1}{T_E(\tau)} \circ D_{\tau_j}G_k(x(t,\tau))\Big) \circ \\ &\Big(D_{\tau_i}\tfrac{1}{T_E(\tau)} \circ G_k(x(t,\tau)) + \tfrac{1}{T_E(\tau)} \circ D_{\tau_i}G_k(x(t,\tau))\Big) + \\ &\Big(\tfrac{1}{T_E(\tau)}G_k(x(t,\tau)) - \phi_k\Big) \circ \\ &\Big(D_{\tau_j}\tfrac{1}{T_E(\tau)}G_k(x(t,\tau)) + \tfrac{1}{T_E(\tau)}D_{\tau_j}D_{\tau_i}G_k(x(t,\tau))\Big)\Big]. \end{aligned} \qquad (16)$$

$D_{\tau_j}G_k(x(t,\tau))$ and $D_{\tau_i}G_k(x(t,\tau))$ are calculated according to Eq. (14). $D_{\tau_j}D_{\tau_i}G_k(x(t,\tau))$ is calculated as follows:

$$\begin{aligned} D_{\tau_j}D_{\tau_i}G_k(\cdot) &= D_1\ell_{k,i}(x(\tau_i),\tau_i) \circ D_{\tau_j}x(\tau_i) \\ &\quad -D_1\ell_{k,i+1}(x(\tau_i),\tau_i) \circ D_{\tau_j}x(\tau_i) \\ &\quad -D_1\ell_k(x(\tau_i),\tau_i) \circ X^i\delta_i^j + \psi_k(\tau_i) \circ X^{i,j} \\ &\quad +\Omega_k(\tau_i) \circ (\Phi(\tau_i,\tau_j) \circ X^j, X^i), \end{aligned} \qquad (17)$$

Where δ_i^j is the Kronecker delta. The first two terms in this expression are the result of differentiating the Leibniz terms from Eq. (14). Evaluating $D_{\tau_j}x(\tau_i)$ depends on the relationship between i and j, as follows:

$$D_{\tau_j}x(\tau_i) = \begin{cases} g_i(x(\tau_i),\tau_i) & i = j \\ \Phi(\tau_i,\tau_j) \circ X^j. & i > j \end{cases}$$

Equation (17) involves the $n \times n$ second-order adjoint $\Omega_k(t)$, which is found by solving the following backwards differential equation:

$$\begin{aligned} \Omega_k(T_f) &= 0_{(n\times n)} \\ \dot{\Omega}_k(t) &= -D_1^2\ell_k(x(t),t) - \psi_k(t) \circ D_1^2 g(x(t),t) - \\ &\quad \Omega_k(t) \circ (D_1 g(x(t),t)) - \Omega_k(t) \circ D_1 g(x(t),t)). \end{aligned} \qquad (18)$$

The terms in $X^{i,j}$ are defined as

$$X^{i,j} = \begin{cases} \begin{array}{c} D_1 g_i(x(\tau_i),\tau_i) \circ g_i(x(\tau_i),\tau_i) + \\ D_1 g_{i-1}(x(\tau_i),\tau_i) \circ g_{i-1}(x(\tau_i),\tau_i) - \\ 2D_1 g_i(x(\tau_i),\tau_i) \circ g_{i-1}(x(\tau_i),\tau_i) + \\ D_2 g_{i-1}(x(\tau_i),\tau_i)) - D_2 g_i(x(\tau_i),\tau_i)) \end{array} & i = j \\ \begin{array}{c} [D_1 g_{i-1}(x(\tau_i),\tau_j) - D_1 g_i(x(\tau_i),\tau_i))] \\ \circ\Phi(\tau_i,\tau j) \circ X^j \end{array} & i > j. \end{cases}$$

Proof: Equation (16) is found by applying the chain rule to (10). $D_{\tau_j}D_{\tau_i}G_k(\cdot)$ can be derived following the same approach as the first derivative, following the derivation in [16]. In this expression, the second order adjoint equation $\Omega_k(t)$ is once again solved K times at each iteration, and evaluated at each transition time. ■

Note: For systems with continuous sampling (i.e. $\ell_1 = \ell_2 = ... = \ell_N$), the equations become somewhat simpler. The total sampling time, $T_E = T_f$, can be treated as a constant and therefore does not need to be differentiated to calculate $D_{\tau_i}J(\cdot)$ and $D_{\tau_j}D_{\tau_i}J(\cdot)$ and the Leibniz terms do not appear in$D_{\tau_i}G(\cdot)$ or $D_{\tau_j}D_{\tau_i}G(\cdot)$.

These equations can also be modified to account for multiple sensing agents, by averaging over agents as well as time, as done in [11].

C. Including Energetic Cost

By including a second term in the cost function, a measure of energetic cost can be included in the optimization as follows:

$$J_W(\tau) = \sum_K \Lambda_k \left|\tfrac{1}{T_E(\tau)}G_k(x(t),t) - \phi_k\right|^2 + \beta W(x(t),t). \qquad (19)$$

In this equation, β is a scaling factor which should be chosen depending on the particular sensing task and energetic constraints of the system. $W(x(t,\tau))$ is a measure of energy loss or work; for physical systems this might be energetic cost for time spent in different modes, or losses due to friction when in contact. This term, when differentiated with respect to a transition time τ_i may involve $D_{\tau_i}x(t)$ and $D_{\tau_j}D_{\tau_i}x(t)$, and therefore involve a second adjoint system derived analogously to Eq (12).

VI. Simulations

Simulations of two example systems and distributions were performed using this algorithm. The first simulation involves a nonlinear system sampling a unimodal distribution, which experiences both contact switches and a directional switch during sampling. The second simulation demonstrates the effects of including the energy loss term in the optimization for a linear system sampling bimodal distributions. All calculations were done using Mathematica.

A. Example 1: Non-linear system sampling a unimodal distribution

In this example a system with four transition times, switching between contact (sampling) and non-contact (non-sampling), is simulated. Recall that there are two aspects of the system that can switch at the transition times: the dynamic equations, and whether or not the segment of the trajectory in that mode is included in the calculations of the basis functions, according to Eq. (6).

In this example, the transition times are calculated to optimally sample a spatial distribution that is a unimodal Gaussian with mean L/2 and variance 0.17. The system dynamics evolve according to

$$\dot{x} = \begin{cases} \frac{1}{4}x(t)^2 & 0 \le t < \tau_1 \quad \text{non-sampling} \\ \frac{1}{4}x(t)^2 & \tau_1 \le t < \tau_2 \quad \text{sampling} \\ -\frac{1}{4}x(t)^2 & \tau_2 \le t < \tau_3 \quad \text{sampling} \\ \frac{1}{4}x(t)^2 & \tau_3 \le t < \tau_4 \quad \text{sampling} \\ \frac{1}{4}x(t)^2 & \tau_4 \le t < 6 \quad \text{non-sampling.} \end{cases}$$

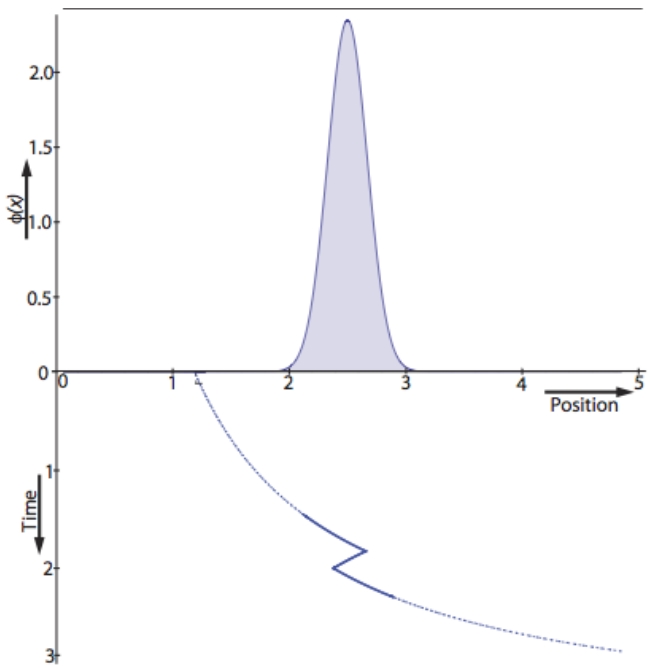

Fig. 2: Distribution and optimal ergodic trajectory calculated for Example 1. The value of the PDF is plotted on the positive vertical axis, the value of time plotted on the negative vertical axis.

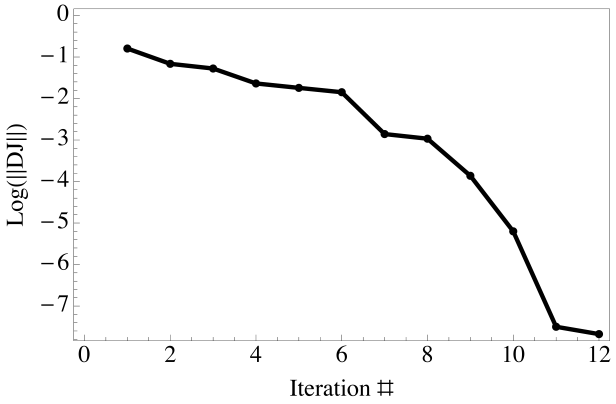

Fig. 3: Logarithmic plot of the norm of the gradient of the cost function for Example 1. The algorithm takes five steps using gradient descent, followed by Newton's method to the optimum. Expected quadratic convergence behavior is apparent; the system converges after only 11 iterations

This distribution and the optimized trajectory are shown in Fig. 2. Energy loss was not included in the objective function for this example. The algorithm was given the initial transition times $\tau = (1.5, 1.8, 2, 2.3)$, and converged to $\tau = (1.4806, 1.8302, 2.0048, 2.2970)$. The optimization demonstrates the expected quadratic convergence behavior using Newton's method, as shown in Fig. 3.

B. Example 2: Kinematic system sampling a bimodal distribution

In this example, several variations on a bimodal distribution are used to demonstrate the results of the algorithm. Optimal trajectories are calculated both with and without including a measure of work loss due to friction in the objective function.

The distribution $\phi(x)$ for this example is defined using a bimodal skew normal distribution as shown below:

$$\begin{aligned} \rho(x) \quad = \quad & \frac{1}{\rho}\left(1+\operatorname{erf}\left(\frac{\alpha_1(x-\zeta_1)}{\sqrt{2}\omega_1}\right)\right)\exp\left(-\frac{(x-\zeta_1)^2}{2\omega_1^2}\right) \\ & +\left(1+\operatorname{erf}\left(\frac{\alpha_2(x-\zeta_2)}{\sqrt{2}\omega_2}\right)\right)\exp\left(-\frac{(x-\zeta_2)^2}{2\omega_2^2}\right) \end{aligned}$$

$$\phi(x) = \frac{\rho(x)}{\int_X \rho(s)ds}.$$

where ζ, ω, and α are the location, scale, and shape parameters, respectively. The simulation was performed over three variations of this distribution, all with $\zeta_1 = 2$, $\zeta_2 = 8$, $\alpha_1 = 5$, $\alpha_2 = -5$. The scale variables ω_1 and ω_2 are varied between three different levels $(0.5, 1.0,$ and $2.0)$ to demonstrate the results of sampling distributions that are very bimodal, moderately bimodal, and nearly flat.

The dynamics $\dot{x}$ and modes for this example are as follows:

$$\dot{x} = \begin{cases} v_1 & 0 \leq t < \tau_1 \quad \text{non-sampling} \\ v_2 & \tau_1 \leq t < \tau_2 \quad \text{sampling} \\ v_1 & \tau_2 \leq t < \tau_3 \quad \text{non-sampling} \\ v_2 & \tau_3 \leq t < \tau_4 \quad \text{sampling} \\ v_1 & \tau_4 \leq t < 6 \quad \text{non-sampling} \end{cases}$$

Although frictional work is taken into account in the cost function, the dynamics assume that an input force is generated in each mode to exactly cancel the frictional force, i.e. $\dot{v} = 0$, and the system can be represented by a single integrator system with constant velocity in each mode. During all five modes in this example, the sampling agent travels in the same direction, and alternates between sampling (experiencing friction) and non-sampling (no friction) modes.

The work loss due to friction during sampling modes will be considered, calculated as

$$W(T_f) = \int_{T_0}^{T_F} w(t,\tau)dt,$$

where

$$w(t,\tau) = \begin{cases} 0 & \text{non-sampling} \\ F_f \cdot \dot{x}(t,\tau) & \text{sampling.} \end{cases}$$

The weighting factor β in Eq. (19) for each distribution was set to be proportional to the scale variable: $\beta = 0.001\omega$.

The three distributions and optimal trajectories for each calculated using an objective function dependent only on ergodicity are plotted in Fig. 4. It can be seen that without minimizing work as well as the distance of the trajectory from being ergodic with respect to the distribution $\phi(x)$, the second and third transition times converge as the distribution flattens out, and the optimal trajectory approaches uniform sampling.

The optimal trajectories calculated using an objective dependent on both work and ergodicity are shown in Fig. 5, as well as the trajectories corresponding to the same distributions without considering energy (the same as shown in Fig. 4). Changing the value of β in Eq. (19) effectively changes how conservatively the distribution is sampled, which adds a degree of flexibility to the algorithm. In some situations, if the distribution is particularly tight (such as the distribution shown in orange in Fig. 4), or if losses due to energy are negligible, the purely ergodic calculations may be desirable. If energetic losses are more critical however, an objective that takes energy into account may be optimal, resulting in a more conservative subset of a distribution being sampled.

VII. Conclusions and Future Work

In order to model the contact decision process during autonomous active tactile exploration, a measure of the ergodicity of a time-averaged trajectory with a spatial distribution is developed as an objective function for transition time optimization. The derivatives with respect to the transition times of the objective are derived for use in first and second order optimization algorithms. Simulations of two example systems are presented which demonstrate that this method is effective in selecting transition times which result in time

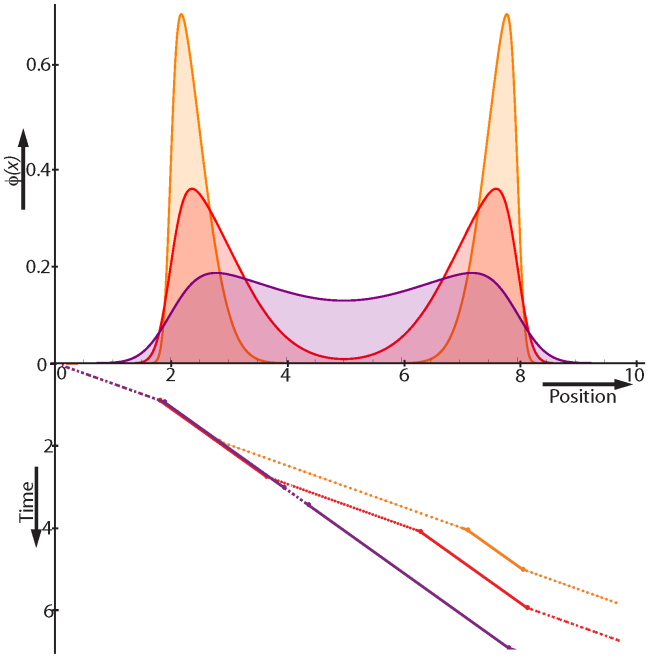

Fig. 4: Optimal trajectories using an ergodic objective function for three different variations of a bimodal distribution. The color of the trajectories indicates which distribution it was optimized with respect to. Modes in which the system is in contact are shown as solid lines, non-contact modes are shown as dotted lines.

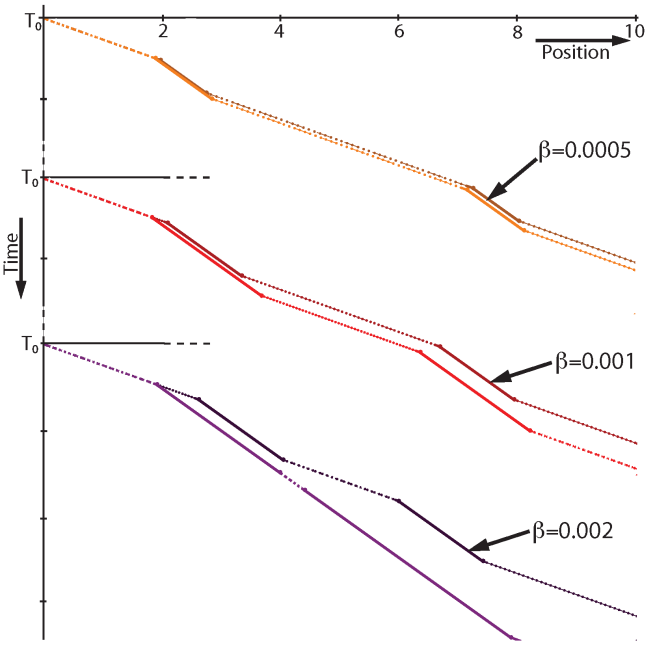

Fig. 5: Optimal trajectories calculated for the same three distributions shown in Fig. 4. For each distribution, the optimal trajectories using an objective that takes ergodicity alone and the optimal trajectory based on both ergodicity and work loss (darker) are shown separately. Color indicates to the distribution sampled. The weighting factor on the work term in Eq. (19), β is indicated for each trajectory

and spatial averages which are optimally ergodic for a given set of dynamics sampling a known distribution. The effect of also considering the weighted losses due to friction during sampling modes was examined as well, generalizing the method to a class of optimal solutions for a particular task.

The simulations in VI-B demonstrate that formulating the contact decision problem as a transition time optimization which uses a measure of ergodicity results in behavior that is qualitatively similar to exploratory behavior carried out by human subjects [2]. As seen in Fig. 4, contact transition times chosen according to an ergodic objective result in trajectories which sample a small area around the peaks of the distribution for very bimodal distributions; trajectories trend towards uniform scanning as the distribution becomes more flat. This behavior is observed in humans. When searching a space with no knowledge of a feature location, uniform scanning behavior is observed. On a second trial for the same task, once the user has some expectation of where a feature is, ballistic motion is observed, followed by sampling of a local area. The authors of [2] leave as an open question whether or not factors such as high surface friction would lead human subjects to resort to ballistic motion during searching even when they have a less reliable internal model due to increased cost of surface scanning. The algorithm provided here provides a reliable way of mathematically taking this effect into account, demonstrating as in Fig. 5 that penalizing surface scanning by examining work loss through friction results in more conservative sampling strategies.

Trials with human subjects are planned in order to characterize if and how energetic cost plays a role in exploratory action, and how this can be used in robotic applications. Future work in this area will involve including the determination of mode order as well as transition times, and applying this algorithm to more complex systems with multiple degrees of freedom and multiple sensing agents. Ultimately, this work can be integrated into a control scheme for autonomous tactile exploration for robotic systems.

ACKNOWLEDGMENT

This material is based upon work supported by the National Institute of Health under grant T32 HD007418 and the National Science Foundation under Grant IIS 1018167. Any opinions, findings, and conclusions or recommendations expressed in this material are those of the author(s) and do not necessarily reflect the views of the National Science Foundation.

REFERENCES

[1] R. Klatzky, S. Lederman, and V. Metzger, "Identifying objects by touch: An expert system," *Attention, Perception, and Psychophysics*, vol. 37, pp. 299–302, 1985.

[2] K. Huynh, C. Stepp, L. White, J. Colgate, and Y. Matsuoka, "Finding a feature on a 3d object through single-digit haptic exploration," in *IEEE Haptics Symposium*, march 2010, pp. 83 –89.

[3] S. J. Lederman and R. L. Klatzky, "Hand movements: A window into haptic object recognition," *Cognitive Psychology*, vol. 19, no. 3, pp. 342 – 368, 1987.

[4] A. Bierbaum, I. Gubarev, and R. Dillmann, "Robust shape recovery for sparse contact location and normal data from haptic exploration," in *IEEE Int. Conf. on Intelligent Robots and Systems (IROS)*, sept. 2008, pp. 3200 –3205.

[5] P. Allen and P. Michelman, "Acquisition and interpretation of 3-d sensor data from touch," *IEEE Transactions on Robotics*, vol. 6, no. 4, pp. 397 –404, aug 1990.

[6] K. Roberts, "Robot active touch exploration: constraints and strategies," in *IEEE Int. Conf. on Robotics and Automation (ICRA)*, may 1990, pp. 980 –985 vol.2.

[7] J. Sinnott and T. Howard, "A hybrid approach to the recovery of deformable superquadric models from 3d data," in *Computer Graphics International 2001. Proceedings*, 2001, pp. 131 –138.

[8] W. E. L. Grimson and T. Lozano-Prez, "Model-based recognition and localization from sparse range or tactile data," *The International Journal of Robotics Research*, vol. 3, no. 3, pp. 3–35, 1984.

[9] A. M. Okamura and M. R. Cutkosky, "Feature detection for haptic exploration with robotic fingers," *The International Journal of Robotics Research*, vol. 20, no. 12, pp. 925–938, 2001.

[10] S. Caselli, C. Magnanini, F. Zanichelli, and E. Caraffi, "Efficient exploration and recognition of convex objects based on haptic perception," in *Robotics and Automation, 1996. Proceedings., 1996 IEEE International Conference on*, vol. 4, apr 1996, pp. 3508 –3513 vol.4.

[11] G. Mathew and I. Mezic, "Metrics for ergodicity and design of ergodic dynamics for multi-agent systems," *Physica D-nonlinear Phenomena*, vol. 240, no. 4-5, pp. 432–442, Feb 2011.

[12] T. Caldwell and T. Murphey, "Switching mode generation and optimal estimation with application to skid-steering," *Automatica*, vol. 47, no. 1, pp. 50 – 64, 2011.

[13] E. Johnson and T. Murphey, "Second-order switching time optimization for nonlinear time-varying dynamic systems," *IEEE Transactions on Automatic Control*, vol. 56, no. 8, pp. 1953 –1957, Aug. 2011.

[14] X. Xu and P. Antsaklis, "Optimal control of switched autonomous systems," in *IEEE Int. Conf. on Decision and Control (CDC)*, vol. 4, dec. 2002, pp. 4401 – 4406.

[15] R. Klatzky, R. Bajcsy, and S. Lederman, "Object exploration in one and two fingered robots," in *Robotics and Automation. Proceedings. 1987 IEEE International Conference on*, vol. 4, mar 1987, pp. 1806 – 1809.

[16] M. Travers, T. Murphey, and L. Pao, "Trajectory optimization estimator for impulsive data association," in *American Controls Conf. (ACC)*, 29 2011-july 1 2011, pp. 4514 –4519.

[17] J. Nocedal and S. Wright, *Numerical Optimization*. Springer, 2006.